

Energy transfer mechanism for downconversion in the (Pr^{3+} , Yb^{3+}) couple

J. T. van Wijngaarden,¹ S. Scheidelaar,¹ T. J. H. Vlugt,² M. F. Reid,³ and A. Meijerink^{1,*}

¹*Debye Institute for Nanomaterials Science, Utrecht University, P.O. Box 80000, 3508 TA Utrecht, The Netherlands*

²*Process & Energy Laboratory, Delft University of Technology, Leeghwaterstraat 44, 2628 CA Delft, The Netherlands*

³*Department of Physics and Astronomy and MacDiarmid Institute for Advanced Materials and Nanotechnology, University of Canterbury, Private Bag 4800, Christchurch 8140, New Zealand*

(Received 22 December 2009; revised manuscript received 22 February 2010; published 15 April 2010)

Downconversion of one visible photon into two infrared photons has been reported for the lanthanide ion couple (Pr^{3+} , Yb^{3+}) in a variety of host lattices. The mechanism responsible for downconversion is controversial and has been reported to be either a two-step energy transfer process (via two first-order transfer steps, the first being cross relaxation) or cooperative energy transfer from Pr^{3+} to two Yb^{3+} ions (a second-order process). Here we report experiments on downconversion for the (Pr^{3+} , Yb^{3+}) in LiYF_4 . Luminescence decay curves of the Pr^{3+} emission are recorded as a function of the Yb^{3+} concentration and analyzed using Monte Carlo simulations for both cooperative energy transfer and energy transfer through cross relaxation. We obtain a good agreement between experiment and simulations for energy transfer by cross relaxation but not for cooperative energy transfer. The observation that cross relaxation is more efficient than cooperative energy transfer is consistent with Judd-Ofelt calculations for the transition probabilities involved in the two energy transfer processes and the lower probability for the second-order cooperative transfer.

DOI: [10.1103/PhysRevB.81.155112](https://doi.org/10.1103/PhysRevB.81.155112)

PACS number(s): 78.20.Bh, 78.47.jd

I. INTRODUCTION

To boost the energy efficiency of solar cells, spectral conversion of the solar spectrum is a promising option.^{1–3} Spectral mismatch losses account for over 60% of the energy losses in a solar cell: low-energy photons are not absorbed (transmission losses) while absorption of high-energy photons is followed by a rapid relaxation of hot charge carriers to the band edges of the semiconductor (thermalization losses).⁴ Lanthanide ions are suitable candidates for efficient spectral conversion. Upconversion (adding two low-energy photons to one give one higher-energy photon) with lanthanides has been studied for decades.⁵ Recent “proof of principle” experiments have demonstrated that it can be used to enhance the solar-cell efficiency.^{6,7}

Work on downconversion (cutting one high-energy photon into two lower-energy photons) is limited in comparison to upconversion studies.⁸ Recently efficient downconversion for solar cells was reported in the (Tb^{3+} , Yb^{3+}) couple.⁹ Following this work, downconversion was reported for a variety of other lanthanide ion couples including (Pr , Yb), (Tm , Yb), and (Er , Yb).^{10–13} Contrary to the detailed studies on the upconversion mechanisms in lanthanide-doped upconversion materials (see, e.g., Ref. 5), research on the downconversion mechanisms is limited. For the (Tb^{3+} , Yb^{3+}) couple the energy transfer mechanism has been established: analysis of the luminescence decay curves of the donor emission (Tb^{3+}) as a function of the acceptor concentration (Yb^{3+}) using Monte Carlo simulations demonstrated that energy transfer occurs through a cooperative dipole-dipole mechanism.⁹ In subsequent papers on downconversion in the (Pr^{3+} , Yb^{3+}) and (Tm^{3+} , Yb^{3+}) couples, it was assumed that here also the energy transfer mechanism was cooperative energy transfer.^{13,14} We reported on efficient downconversion for the (Pr , Yb) couple in SrF_2 and indicated that for this couple a resonant two-step energy transfer process is more probably

than the second-order cooperative energy transfer process.¹¹ However, no convincing evidence for either mechanism has been reported. In Fig. 1 the two processes are depicted schematically: in case of cooperative energy transfer from the $^3\text{P}_0$ level of the Pr^{3+} donor, the energy is transferred to two neighboring Yb^{3+} acceptors in a single step [Pr^{3+} ($^3\text{P}_0 \rightarrow ^3\text{H}_4$); 2 Yb^{3+} ($^2\text{F}_{7/2} \rightarrow ^2\text{F}_{5/2}$)]. In case of resonant two-step energy transfer, first part of the energy is transferred to one Yb^{3+} neighbor through cross relaxation [Pr^{3+} ($^3\text{P}_0 \rightarrow ^1\text{G}_4$); Yb^{3+} ($^2\text{F}_{7/2} \rightarrow ^2\text{F}_{5/2}$)] followed by a second energy transfer step [Pr^{3+} ($^1\text{G}_4 \rightarrow ^3\text{H}_4$); Yb^{3+} ($^2\text{F}_{7/2} \rightarrow ^2\text{F}_{5/2}$)]. Valid arguments were provided for both mechanisms: the relatively weak dipole oscillator strength of the $^3\text{P}_0 \rightarrow ^1\text{G}_4$ transition may prevent the cross-relaxation step. On the other hand, a second-order process for energy transfer is typically 10^3 less probable than a first-order process which gives cooperative energy transfer a low probability. Indeed, for the Tb , Yb couple efficient energy transfer was only observed for high Yb^{3+} acceptor concentrations.⁹

It is the aim of this paper to elucidate the energy transfer mechanism for downconversion in the (Pr , Yb) couple. To do this, the luminescence decay curves of the donor emission ($^3\text{P}_0$ emission from Pr^{3+}) were measured as a function of the acceptor (Yb^{3+}) concentration and analyzed, both with analytical solutions and with Monte Carlo simulations. As a model system LiYF_4 was chosen as host lattice. The relatively high symmetry (Scheelite structure) of this host makes it simpler to model the acceptor configurations around the donor. Modeling of the decay curves demonstrates that the dominant mechanism for energy transfer from the $^3\text{P}_0$ level of Pr^{3+} to Yb^{3+} is cross relaxation via dipole-dipole interaction and not cooperative energy transfer. The relaxation rates are proportional to the dipole strengths of the $^3\text{P}_0 \rightarrow ^1\text{G}_4$ and $^3\text{P}_0 \rightarrow ^3\text{H}_4$ transitions. We used Judd-Ofelt theory to determine the ratios of these two dipole strengths. The $^3\text{P}_0 \rightarrow ^1\text{G}_4$ dipole strength is estimated to be a factor of 20

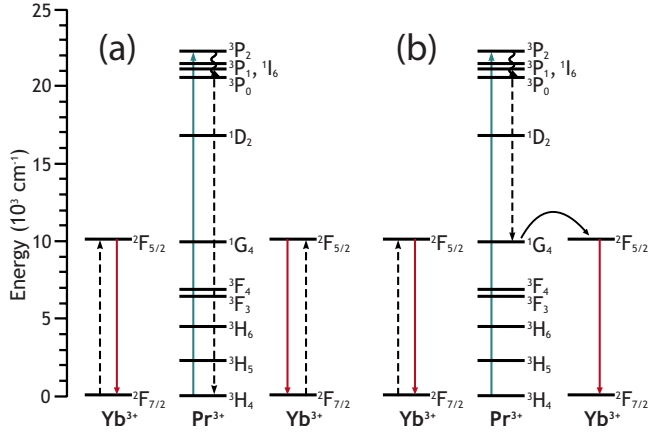


FIG. 1. (Color online) Energy level scheme and downconversion mechanism for the (Pr³⁺, Yb³⁺) couple. (a) shows the cooperative energy transfer where the energy is simultaneously transferred to two Yb³⁺ ions. (b) shows first-order energy transfer where the energy is stepwise transferred to Yb³⁺ ions, using the ¹G₄ level as an intermediate state. Dotted arrows represent nonradiative energy transfer and solid arrows are optical transitions.

smaller than the ³P₀ → ³H₄ dipole strength. However it would have to be a factor of 1000 smaller for the cooperative process to be competitive with cross relaxation since the cooperative is a second-order effect.

II. EXPERIMENTAL

Crystalline powder samples were prepared of LiYF₄:Pr³⁺ (0.5%) co-doped with Yb³⁺ (0%, 2%, 5%, 10%, 20%, and 40%) by solid-state techniques. LiF (5% molar excess), PrF₃, YbF₃, and YF₃ were thoroughly mixed and NH₄F was added to create a fluoride environment in the atmosphere to reduce the incorporation of oxygen in the lattice. We then annealed the samples at 675 °C in a nitrogen atmosphere. The crystal structure of the samples was checked with x-ray powder diffraction. The XRD patterns show no evidence for the presence of a second crystalline phase (such as oxyfluorides) which indicates that within the detection limit of XRD (~1%) the samples are phase pure.

Diffuse reflectance spectra were recorded using a spectrometer with an integrating sphere (Perkin-Elmer Lambda 950). We measured emission spectra on a SPEX DM3000F spectrofluorometer with a 450 W xenon lamp with a 0.22 m excitation monochromator for excitation while the emission was detected with a Princeton Instruments 300i charge coupled device detector coupled to a 0.3 m Acton Research monochromator. Excitation spectra were measured with an Edinburgh Instruments FLS 920 spectrofluorometer with a Hamamatsu R928 photomultiplier tube (PMT) for the 400–800-nm wavelength range or a liquid-nitrogen-cooled Hamamatsu R5509–72 PMT for the 800–1600-nm range. Luminescence decay curves were measured under pulsed excitation with a LPD3000 dye laser (Coumarin 102 dye, 481 nm) pumped by a Lambda Physik LPX excimer laser (XeCl, 308 nm). The decay traces were recorded with a digital oscilloscope (Tektronix 2440).

III. MODELING

The variation of luminescence decay curves for the donor emission as a function of the acceptor concentration is strongly dependent on the energy transfer mechanism.⁹ In case of first order energy transfer by cross relaxation through dipole-dipole interaction, the energy transfer rate from the Pr³⁺ ion in the ³P₀ excited state will show a 1/*r*_{*i*}⁶ distance dependence for transfer to every Yb³⁺ acceptor *i* in the surroundings. In case of cooperative energy transfer through dipole-dipole interaction, the distance dependence is more complicated and follows a 1/(*r*_{*i*}⁶*r*_{*j*}⁶) dependence to every pair (*i*, *j*) of Yb³⁺ acceptors around the Pr³⁺ donor. To model the experimentally measured decay curves for the different Yb³⁺ concentrations, Monte Carlo simulations were used to randomly create possible surroundings of Yb³⁺ acceptors around the Pr³⁺ donor. The LiYF₄ unit cell (Scheelite structure, with *a*=*b*=5.164 Å and *c*=10.741 Å) and the positions of the Y ions in the unit cell serve as input. The size of the simulation box was 8 times 8 times 4 (=256) unit cells. According to the nearest image convention all interactions up to 20.66 Å are considered. We considered 20 000 random realizations in each simulation and verified that this was sufficient.

The methodology we used for the modeling has been described in detail in Ref. 9. For each configuration (which is a specific distribution of Yb³⁺ acceptors at distances *r*_{*i*} around the Pr³⁺ donor) the decay is given by a single exponential

$$I(t) = \exp[-t(\gamma_r + \gamma_{tr})]. \quad (1)$$

Here *t* is the time, γ_r is the radiative decay rate of the ³P₀ state of Pr³⁺ in LiYF₄ and γ_{tr} is the energy transfer rate to all Yb neighbors at distances *r*_{*i*}. For single-step energy transfer via dipole-dipole interaction, the transfer rate is given by

$$\gamma_{tr} = C_{cr} \sum_i \frac{1}{r_i^6}. \quad (2)$$

*C*_{*cr*} is a fitting parameter for energy transfer by cross relaxation through dipole-dipole interaction. In case of energy transfer through the cooperative dipole-dipole mechanism, the transfer rate from the Pr³⁺ donor to a pair of Yb³⁺ acceptors, at distances *r*_{*i*} and *r*_{*j*} is given by

$$\gamma_{tr} = C_{coop} \sum_{i < j} \frac{1}{r_i^6 r_j^6}. \quad (3)$$

*C*_{*coop*} is a fitting parameter for energy transfer through cooperative energy transfer via dipole-dipole interaction.

The experimental decay curves result from an ensemble average of the different configurations. Therefore an ensemble average signal is calculated:

$$\langle I(t) \rangle = \exp[-t(\gamma_r + \gamma_{tr})], \quad (4)$$

where $\langle \rangle$ denotes ensemble averaging over 20 000 configurations. The equations given here are equivalent to the description in Ref. 9. The equations for single-step energy transfer through cross relaxation correspond to what was labeled phonon assisted in Ref. 9. Since in case of energy transfer from Tb³⁺ to Yb³⁺ the large energy mismatch would require (multi-) phonon assistance to make up for the energy

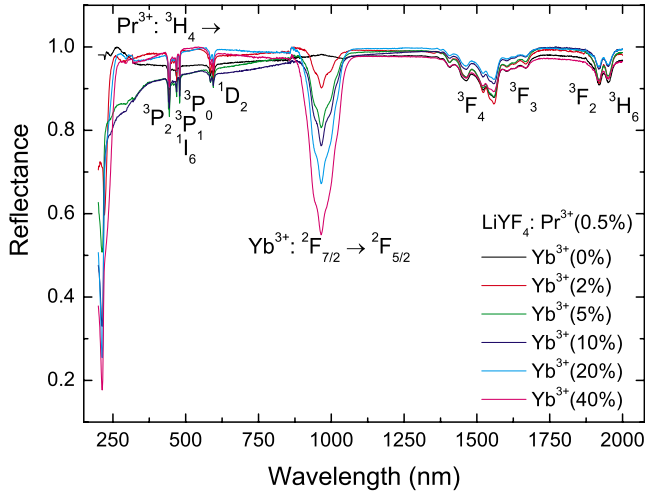


FIG. 2. (Color online) Diffuse reflectance spectra of $\text{LiYF}_4:\text{Pr}^{3+}, \text{Yb}^{3+}$ (0%, 2%, 5%, 10%, 20%, and 40%).

mismatch. For the $[\text{Pr}^{3+} {}^3\text{P}_0 \rightarrow {}^1\text{G}_4; \text{Yb}^{3+} {}^2\text{F}_{7/2} \rightarrow {}^2\text{F}_{5/2}]$ cross-relaxation process there is no need for phonon assistance and resonant energy transfer with the same $1/r^6$ distance dependence is expected.

To compare the experimentally observed decay curves for the different Yb^{3+} concentrations with the simulated curves, we fitted the decay curves observed for the sample with 2% Yb^{3+} . The parameters obtained were used to simulate the decay curves for all other concentrations (without further fitting).

In addition to modeling using Monte Carlo simulations, also a fitting procedure using analytical solutions was done. The same expressions for the transfer rate were used as for the Monte Carlo simulations. The probability for a certain configuration was not obtained through the averaging by Monte Carlo simulations but calculated assuming a statistical distribution of the acceptor ions. From the crystal structure of LiYF_4 it is possible to calculate the number of Yb^{3+} ions in each shell at distance r_i around the donor ion. The probability for a specific configuration with n Yb^{3+} ions in the various shells is given by

$$P_{conf} = \prod_{Sh} \frac{N_{Sh}!}{(N_{Sh} - n_{Yb})! n_{Yb}!} c_{Yb}^{n_{Yb}} (1 - c_{Yb})^{N_{Sh} - n_{Yb}}. \quad (5)$$

The product runs over all shell surrounding the Pr^{3+} ion, c_{Yb} is the fraction of Yb^{3+} ions, N_{Sh} is the number of rare-earth sites in the shell and n_{Yb} is the number of Yb^{3+} ions in this shell. In the fits to the analytical expressions, the number of shells included was varied between 2 and 7. The nearest-neighbor shell includes four neighbors at 3.7 Å up while the seventh shell has also four neighbors at 8.5 Å.

IV. RESULTS AND DISCUSSION

Diffuse reflectance spectra (Fig. 2) show that the absorption peaks corresponding to Pr^{3+} transitions (for example, the ${}^3\text{H}_4 \rightarrow {}^3\text{P}_j$ between 440 and 500 nm) have similar absorption strength for the various samples. This indicates that the Pr^{3+}

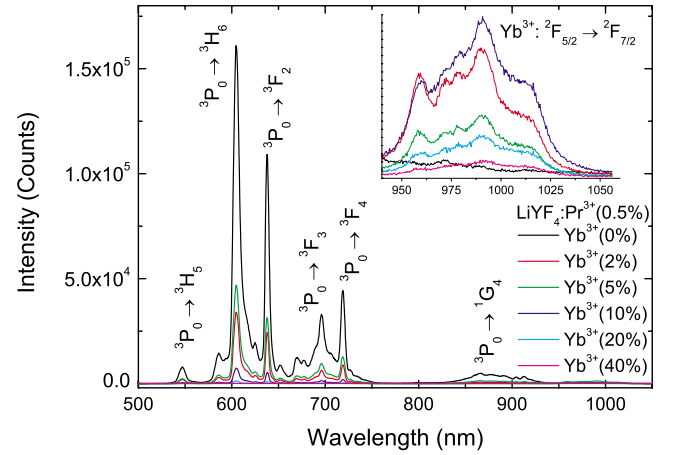


FIG. 3. (Color online) Emission spectra for $\text{LiYF}_4:\text{Pr}^{3+}, \text{Yb}^{3+}$ (0%, 2%, 5%, 10%, 20%, and 40%). Spectra were recorded at room temperature and excited at 481 nm. The inset shows a magnification of the Yb^{3+} luminescence around 1000 nm.

concentration is the same in all samples. The absorption strength for to the Yb^{3+} transition around 1000 nm increases with increasing Yb^{3+} concentration, as expected. The strong absorption band below 250 nm is probably due to an $\text{O}^{2-} - \text{Yb}^{3+}$ charge transfer absorption band. In a fluoride compound oxygen is a common impurity. The position of the absorption band is consistent with the typical energy for an $\text{O}^{2-} - \text{Yb}^{3+}$ charge transfer band. Also the observation that the absorption strength increases with Yb^{3+} concentration supports the assignment. In longer wavelength region a weaker broadband absorption is observed below 400 nm for the samples co-doped with 5 and 10% Yb^{3+} . The origin is not clear and may be defect absorption. Since the absorption partly overlap with the Pr^{3+} absorption lines around 450 nm, it may reduce the luminescence efficiency when exciting at these wavelengths.

Figure 3 shows emissions spectra for samples with Yb^{3+} concentration varying from 0% to 40%, collected at room temperature under excitation at 481 nm. The spectra are not corrected for the detector response. For low Yb^{3+} concentrations the spectra show characteristic Pr^{3+} emission lines which are well known for this compound.¹⁵ Upon increasing the Yb^{3+} concentration the Pr^{3+} emission intensity decreases and at 40% Yb^{3+} concentration hardly any Pr^{3+} emission is observed. This indicates efficient energy transfer to Yb^{3+} . Indeed, Yb^{3+} emission is observed in the co-doped samples around 1000 nm. The inset in Fig. 3 shows this region magnified with clear Yb^{3+} emission peaks. The highest emission intensity is observed for the sample co-doped with 10% Yb^{3+} . For higher Yb^{3+} concentrations the emission intensity decreases which we ascribe to concentration quenching. Quenching of the Yb^{3+} emission is enhanced by multiphonon relaxation due to coupling with the high-energy OH^- vibrations of OH^- groups present in the samples as an impurity. At higher Yb^{3+} concentrations energy migration to Yb^{3+} next to OH^- groups will contribute significantly to concentration quenching.

Further evidence for energy transfer is obtained from Fig. 4, which shows excitation spectra. The emissions monitored

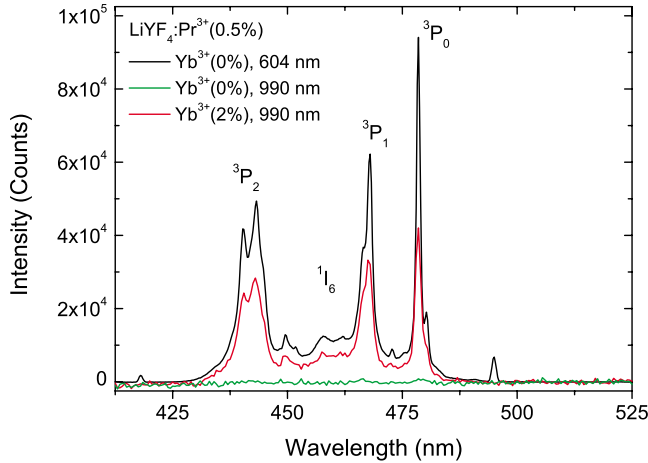


FIG. 4. (Color online) Excitation spectra for $\text{LiYF}_4:\text{Pr}^{3+}, \text{Yb}^{3+}$ (0% and 2%). The emissions monitored are: $\text{Pr}^{3+} \ ^3\text{P}_0 \rightarrow \ ^3\text{H}_6$ at 604 nm and the $\text{Yb}^{3+} \ ^2\text{F}_{5/2} \rightarrow \ ^2\text{F}_{7/2}$ at 990 nm.

are the $\text{Pr}^{3+} \ ^3\text{P}_0 \rightarrow \ ^3\text{H}_6$ at 604.5 nm (only the 0% Yb^{3+} sample) and the $\text{Yb}^{3+} \ ^2\text{F}_{5/2} \rightarrow \ ^2\text{F}_{7/2}$ at 990 nm, for 0% and 2% Yb^{3+} concentration. It is clear from these spectra that for the 2% Yb^{3+} sample, we observe Yb^{3+} emission upon excitation in $\text{Pr}^{3+} \ ^3\text{P}_j$ and $^1\text{I}_6$ levels between 440 and 500 nm. The luminescence spectra show that efficient energy transfer occurs but does not provide direct information on the energy transfer mechanism.

To get insight in the energy transfer mechanism, we recorded luminescence decay curves for the Pr^{3+} emission. Figure 5 (dots) shows these decay curves for the $\text{Pr}^{3+} \ ^3\text{P}_0 \rightarrow \ ^3\text{H}_6$ emission at 606 nm upon excitation at 481 nm. For 0% Yb^{3+} concentration the decay curve is close to single exponential with a $\sim 36 \mu\text{s}$ decay time. This is in agreement with the room-temperature lifetime of $35.7 \mu\text{s}$ reported for the $^3\text{P}_0$ emission in LiYF_4 doped with 0.65% Pr^{3+} .¹⁵ A slight

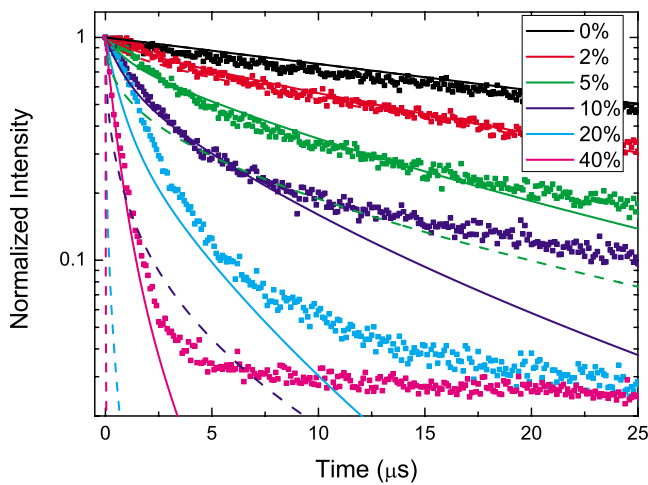


FIG. 5. (Color online) Luminescence decay curves of the $^3\text{P}_0 \rightarrow \ ^3\text{H}_6$ emission of Pr^{3+} in $\text{LiYF}_4:\text{Pr}^{3+}, \text{Yb}^{3+}$ (0%, 2%, 5%, 10%, 20%, and 40%) at 606 nm. The experimental data (dots) are measured under pulsed laser excitation at 481 nm. The solid line is the simulated decay for phonon-assisted energy transfer and the dashed line is the simulated decay for cooperative energy transfer.

TABLE I. Parameters used in the Monte Carlo simulations and the analytical calculations.

	γ_r (ms^{-1})	C^a
Cross relaxation	17.95	2.6×10^6
Cooperative	17.95	1.5×10^6

^aUnits for cross relaxation $\text{ms}^{-1} \text{ \AA}^{-6}$ and for cooperative mechanism $\text{ms}^{-1} \text{ \AA}^{-12}$.

deviation from single-exponential decay is ascribed to cross relaxation between Pr^{3+} neighbors, which already occur at this low concentration. The observation of a close-to-single exponential decay with a decay time that is consistent with the radiative lifetimes reported in literature shows that impurities (O^{2-} or OH^-) do not significantly influence the decay curves. This also shows that the decay curves of the $^3\text{P}_0$ emission can be used to analyze energy transfer to neighboring Yb^{3+} ions.

Upon co-doping with Yb^{3+} , the decay becomes nonexponential and faster. This is consistent with efficient energy transfer from the $^3\text{P}_0$ level of Pr^{3+} to Yb^{3+} neighbors.

From the evolution of the decay traces with increasing Yb^{3+} concentration the operative energy transfer mechanism can be deduced. The experimentally measured decay curves were simulated using Monte Carlo simulations [Eq. (4)] where γ_{tr} was determined for both cross-relaxation [Eq. (2)] and cooperative energy transfers [Eq. (3)]. In Fig. 5 the solid lines present the best fit obtained for energy transfer via cross relaxation and the dashed lines represent the best fits obtained for cooperative energy transfer. The colors correspond to the different Yb^{3+} concentrations and the fitted curves should overlap with the experimental curves of the same colors. The fit parameters are tabulated in Table I.

Comparison of the experimentally measured decay curves and the fitted curves show that for 0% and 2% Yb^{3+} concentration both mechanisms fit the data fairly well. For higher concentrations only the cross-relaxation model gives a good description of the experimentally observed decay curves. For the 0% and 2% the good agreement is obvious: for 0% in both models the decays are described by the radiative decay (no contribution from energy transfer) and the decay curves for the 2% Yb^{3+} were used to determine the fit parameters C_{cr} and C_{coop} . We used these fit parameters to simulate the decay curves for the higher Yb^{3+} concentrations. The simulated decay curves based on energy transfer via cross relaxation describe the experimentally observed decay behavior quite well for all Yb^{3+} concentrations. The decay curves simulated for energy transfer via cooperative energy transfer strongly deviate from the experimentally observed decay. Clearly, the value obtained for C_{coop} needed to describe the energy transfer through cooperative energy transfer for this low Yb^{3+} concentration, is high and results in very efficient cooperative energy transfer upon raising the Yb^{3+} concentration.

The good agreement obtained between the simulation using the cross-relaxation mechanism and experimental results shows that the operative energy transfer mechanism is cross

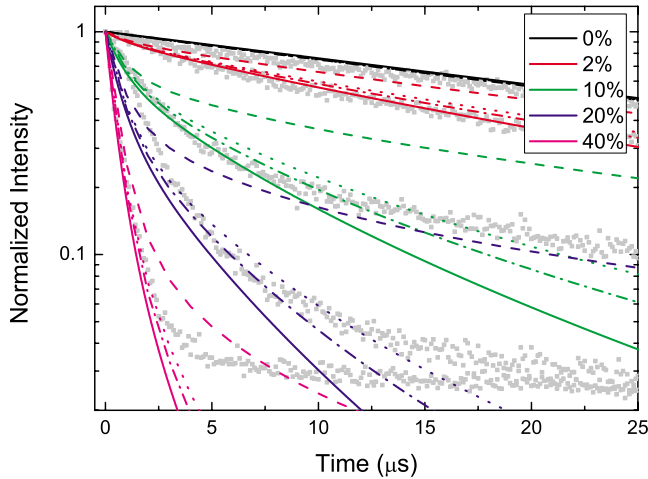


FIG. 6. (Color online) Luminescence decay curves of the ${}^3P_0 \rightarrow {}^3H_6$ emission of Pr^{3+} in $\text{LiYF}_4:\text{Pr}^{3+}, \text{Yb}^{3+}$ (0%, 2%, 10%, 20%, and 40%) at 606 nm. The gray dots are experimental curves and the solid lines represent the simulated decay curves for the phonon-assisted energy transfer. The dashed, dotted, and dashed dotted line are analytical calculations including two, four, and seven shells, respectively.

relaxation, which shows that downconversion occurs through resonant two-step energy transfer and not cooperative energy transfer. At high concentrations there may also be a contribution from resonant energy transfer to a real excited state of an exchange coupled Yb^{3+} pair. This specific type of energy transfer has not been included in the analysis since we do not have a good model to do this and previous results show that the cooperative mechanism describes the data well in $(\text{Y}, \text{Yb})\text{PO}_4$, even at the highest concentrations.⁹

Figure 6 shows the results of the analytical calculations, where we used the probability distribution function [Eq. (5)], to calculate the distribution of the Yb^{3+} ions for given concentrations. The energy transfer rate was calculated only for the first-order mechanism [Eq. (2)]. For comparison we also plotted the experimental data (gray dots) and the Monte Carlo simulations for the first-order energy transfer. The dashed, dotted, and dashed-dotted lines are analytical results including two, four, and seven shells, respectively, and the colors represent different Yb^{3+} concentrations. There is a large difference between the analytical calculated results and the Monte Carlo simulated results, when only two shells are included. Including more shells rapidly improves the results but there is still significant difference between the analytical and Monte Carlo simulated results when seven shells are included. This indicates that energy transfer over longer distances (over 8.5 Å, the distance to neighbors in the seventh shell) is not negligible and contributions to the observed decay behavior. Especially in the longer time regime where slow energy transfer to distant neighbors is observed.

As was stated in the introduction, there have been valid arguments for both first-order and cooperative energy transfer in the $(\text{Pr}^{3+}, \text{Yb}^{3+})$ couple. We will take a closer look at these arguments here. If energy transfer through cross relaxation occurs, the first step in this process is the $\text{Pr}^{3+} {}^3P_0 \rightarrow {}^1G_4$ transition. However this transition has a weak dipole

TABLE II. Reduced matrix elements for all the possible transitions from the 3P_0 level and the relative intensities. We have set the highest intensity at 100.

${}^3P_0 \rightarrow$	$(U^{(2)})^2$	$(U^{(4)})^2$	$(U^{(6)})^2$	Relative intensity
1D_2	0.0168	0	0	0
1G_4	0	0.0520	0	4.36
3F_4	0	0.110	0	19.3
3F_3	0	0	0	0
3F_2	0.296	0	0	0
3H_6	0	0	0.07272	27.2
3H_5	0	0	0	0
3H_4	0	0.173	0	100

oscillator strength, which can be calculated with the Judd-Ofelt theory.^{16,17} For the calculations the $U^{(\lambda)}$ ($\lambda=2,4,6$) reduced matrix elements for the various transitions are needed. Unfortunately, the well-known tables published by Carnall *et al.*¹⁸ of reduced matrix elements do not include the reduced matrix elements for the ${}^3P_0 \rightarrow {}^1G_4$ transition. We therefore calculated the reduced matrix elements for all transitions from the 3P_0 level and Table II gives the calculated reduced matrix elements $(U^{(\lambda)})^2$ for the 3P_0 transitions in Pr^{3+} .

Using the Judd-Ofelt parameters for Pr^{3+} in LiYF_4 ($\Omega_2=0$, $\Omega_4=8.07 \times 10^{-20} \text{ cm}^{-2}$, and $\Omega_6=7.32 \times 10^{-20} \text{ cm}^{-2}$) from the literature,¹⁹ we calculated the relative intensities of the transitions. From these relative intensities it follows that the ${}^3P_0 \rightarrow {}^3H_4$ transition is more than 20 times more probable than the ${}^3P_0 \rightarrow {}^1G_4$ transition. To understand what the dominant energy transfer process will be, one must also take into account the different probabilities of the different mechanisms. First-order energy transfer processes are typically 10^3 times more probable than second-order processes.⁵ Thus for the cooperative process to be competitive with the cross-relaxation process, the difference in dipole strength must be a factor 1000 instead of the factor 20 that we have calculated. The fact that we observe energy transfer through a first-order dipole-dipole cross-relaxation process is therefore consistent with theory.

V. CONCLUSIONS

We have studied the energy transfer mechanism for downconversion in the $(\text{Pr}^{3+}, \text{Yb}^{3+})$ couple in LiYF_4 . Luminescence decay curves of the donor emission were recorded for varying acceptor concentrations. We compared the decay traces with simulated decay curves for both first- and second-order energy transfers, using Monte Carlo simulations. This shows that first-order energy transfer by cross relaxation is the dominant energy transfer mechanism and not cooperative energy transfer. Analytical calculations of the decay curves confirm the results from the simulations. Evaluation of the Judd-Ofelt theory shows that the ${}^3P_0 \rightarrow {}^1G_4$ transition, essential for cross relaxation, has a low oscillator strength which reduces the cross-relaxation rate, but this is compensated by the 10^3 times higher probability for first-order energy transfer, compared to cooperative energy transfer.

ACKNOWLEDGMENTS

This work is part of the Joint Solar Programme (JSP) of the Stichting voor Fundamenteel onderzoek der Materie

(FOM), which is part of the Nederlandse Organisatie voor Wetenschappelijk onderzoek (NWO). The JSP is cofinanced by gebied Chemische Wetenschappen of NWO and stichting Shell Research.

*a.meijerink@uu.nl

- ¹T. Trupke, M. A. Green, and P. Würfel, *J. Appl. Phys.* **92**, 4117 (2002).
- ²T. Trupke, M. A. Green, and P. Würfel, *J. Appl. Phys.* **92**, 1668 (2002).
- ³T. Trupke, A. Shalav, B. S. Richards, P. Würfel, and M. A. Green, *Sol. Energy Mater. Sol. Cells* **90**, 3327 (2006).
- ⁴W. Shockley and H. Queisser, *J. Appl. Phys.* **32**, 510 (1961).
- ⁵F. Auzel, *Chem. Rev.* **104**, 139 (2004).
- ⁶P. Gibart, F. Auzel, J. C. Guillaume, and K. Zahraman, *Jpn. J. Appl. Phys.* **35**, 4401 (1996).
- ⁷A. Shalav, B. Richards, T. Trupke, and H. Güdel, *Appl. Phys. Lett.* **86**, 013505 (2005).
- ⁸R. T. Wegh, H. Donker, K. D. Oskam, and A. Meijerink, *Science* **283**, 663 (1999).
- ⁹P. Vergeer, T. J. H. Vlugt, M. H. F. Kox, M. I. den Hertog, J. P. J. M. van der Eerden, and A. Meijerink, *Phys. Rev. B* **71**, 014119 (2005).
- ¹⁰L. Aarts, B. M. van der Ende, and A. Meijerink, *J. Appl. Phys.* **106**, 023522 (2009).
- ¹¹B. M. van der Ende, L. Aarts, and A. Meijerink, *Adv. Mater.* **21**, 3073 (2009).
- ¹²L. Xie, Y. Wang, and H. Zhang, *Appl. Phys. Lett.* **94**, 061905 (2009).
- ¹³Q. Zhang, G. Yang, and Z. Jiang, *Appl. Phys. Lett.* **91**, 051903 (2007).
- ¹⁴D. Chen, Y. Wang, Y. Yu, P. Huang, and F. Weng, *Opt. Lett.* **33**, 1884 (2008).
- ¹⁵F. Cornacchia, A. Di Lieto, M. Tonelli, A. Richter, E. Heumann, and G. Huber, *Opt. Express* **16**, 15932 (2008).
- ¹⁶B. R. Judd, *Phys. Rev.* **127**, 750 (1962).
- ¹⁷G. S. Ofelt, *J. Chem. Phys.* **37**, 511 (1962).
- ¹⁸W. T. Carnall, H. Crosswhite, and H. M. Crosswhite, *Energy Level Structure and Transition Probabilities of the Trivalent Lanthanides in LaF₃* (Argonne National Laboratory, Argonne, IL, 1977).
- ¹⁹J. L. Adam, W. A. Sibley, and D. R. Gabbe, *J. Lumin.* **33**, 391 (1985).